# The seismic performance of end-perforated RC frame beams strengthened with CFRP sheets

Qianjin Shu[1] Guanglin Yuan[2], Zhaohui Huang[3], Limin Lu [4], Xu He [5]

1 PhD, Lecturer, State Key Laboratory for Geomechanics & Deep Underground Engineering, School of Mechanics & Civil Engineering, China University of Mining & Technology, Xuzhou, Jiangsu 221116, China.

2 PhD, Professor, State Key Laboratory for Geomechanics & Deep Underground Engineering, School of Mechanics & Civil Engineering, China University of Mining & Technology, Xuzhou, Jiangsu 221116, China.

3 PhD, Reader, Department of Civil & Environmental Engineering, Brunel University, Uxbridge, Middlesex, UB8 3PH, UK. (corresponding author: zhaohui.huang@brunel.ac.uk)

4 PhD, Lecturer, State Key Laboratory for Geomechanics & Deep Underground Engineering, School of Mechanics & Civil Engineering, China University of Mining & Technology, Xuzhou, Jiangsu 221116, China.

5 MSc, Research Student, State Key Laboratory for Geomechanics & Deep Underground Engineering, School of Mechanics & Civil Engineering, China University of Mining & Technology, Xuzhou, Jiangsu 221116, China.

**Abstract**: This paper presents eight tests on the end-perforated RC frame beams with the different sizes of perforations and arrangement styles of strengthening carbon fibre (CFRP) sheets subjected to hybrid load-displacement control loading condition. The research focuses on the assessment of beams' seismic performance. The ultimate load resistance, hysteretic performance, energy dissipation capability, ductility and stiffness degradation of the end-perforated RC frame beams with and without strengthening CFRP sheets have been investigated. The test results show that the beams strengthened with CFRP sheets can effectively improve their seismic performances. The perforation size of a beam has significant influence on its seismic behaviour. With the increase of hole diameter, the hysteresis performance, energy dissipation capacity and ductility of beams are decreased considerably.

**Keywords**: Beams & girders; Concrete structures; Strength & testing of materials.

## 1. Introduction

In building construction sometimes it is needed to make holes in the webs of RC beams in order to pass some service pipes. However, the holes weaken the integrity, shear resistance and seismic performance of beams (Douglas and Gambrell 1974; Mansur et al. 1985; Wang et al. 2011; Aykac et al. 2014; Xue and Zheng 2014). In recent years, a considerable amount of research has been conducted to investigate the mechanical performance of the perforated beams with different strengthening methods under normal design loading conditions. For example: Xue and Zheng (2014) studied the mechanical behaviour of the perforated beams strengthened with various steel bars surrounding the holes. Aykac et al. (2014) investigated the influences of different parameters, such as the shape of perforation, stirrups between perforations, diagonal steel bars and the ratio of longitudinal steel bars, on the bending resistance of the beams. Mansur et al. (1985) tested a number of perforated beams to analyse the ultimate resistance of the beams. Mansur et al. (1991) conducted the tests on eight continuous RC beams with rectangular perforations and proposed a method to predict the load-deflection relationship of the beams.

Grace and Ross (1996) studied the dynamic behaviour of the perforated post-stressed RC beams with rectangular T and I sections under cyclic loading without any strengthening. Anil (2008) performed an experimental study on the shear insufficient RC beams strengthened with carbon fibre (CFRP) sheets under cyclic loading. Ahmed et al. (2012) conducted a review on the structural characteristics of the perforated beams with variations on perforation position, shape of opening, the relevant design methods, and the researches on strengthening the openings with fibre materials, steel plates, etc. El-Maaddawy and El-Ariss (2012) carried out the tests on sixteen perforated beams strengthened with CFRP sheets, and analysed the effects of strengthening on the shear resistance and stiffness of the beams. Zhang and Hsu (2005) reported that CFRP sheets could significantly improve the ductility and ultimate shear resistance of beams.

Previous research indicated that for strengthening the perforations of RC beams CFRP sheets have advantages of high strength, low self-weight, ease of construction, shortened construction period, etc. As the literature review presented above the most reported researches on perforated beams were

focused on the structural behaviours of the beams under normal design loading conditions. The research on the seismic performance of the perforated RC beams strengthened with CFRP sheets is limited. Hence, the aim of this research is to experimentally study the seismic performance of the perforated RC beams strengthened with CFRP sheets. The main objectives of the research are:

- Conduct the tests of eight end-perforated RC frame beams with the different sizes of perforations and arrangement styles of strengthening CFRP sheets to assess their seismic performance using hybrid load-displacement control loading method.
- Investigate the ultimate load resistance, hysteretic performance, energy dissipation capability, and ductility and stiffness degradation of the end-perforated RC frame beams with and without the strengthening CFRP sheets.
- Generate some valuable test data for enhancing the earthquake resistance design of the end-perforated RC frame beams using CFRP sheets.

## 2. Experimental program

### *2.1 Specimen design*

In this experimental study, eight RC beams were designed for the tests. The beam specimen was assumed to represent the part between the joint of beam-column to the mid-span of the beam within a planar RC frame. The dimensions of cross sections were 150 mm×300 mm for beams, and 300 mm×400 mm for columns. Table 1 and Fig. 1 give the details of the beam specimens. Beam LA0 was intact without perforation for the purpose of reference. Beams LA1, LA2 and LA3 were the perforated beams without CFRP sheets strengthening. Other four beams in group B were the perforated beams with CFRP strengthening.

Normal strength concrete, C25, was used for all beams. The tested compressive strength of concrete at 28 day was 28.5 MPa. As shown in Fig. 1, the stirrup of beam and column had the diameter of 6 mm and spacing of 100 mm. The main reinforcing steel bar had the diameter of 18 mm. The tested material properties of reinforcement are listed in Table 2.

In this research HITEX-C300 carbon fibre (CFRP) sheet (produced by Nanjing Haituo Composite

Material Ltd) was used. The material properties of CFRP sheets were: unit weight = 300g/$m^2$, thickness = 0.167 mm, tensile strength = 4330 MPa, elastic modulus = $2.56\times10^5$ MPa, elongation = 1.7%. The structural adhesive glue used was Lica-100 modified epoxy resin. The properties of the glue were: tensile strength = 40 MPa, tensile modulus = 2500 MPa, compressive strength = 70 MPa, bending strength = 50 MPa, elongation = 1.5%.

Two strengthening methods were employed for the perforated beams: (1) horizontal arrangement (Fig. 2 and Fig. 4(a)); (2) 45° diagonal arrangement (Fig. 3 and Fig. 4(b)). The amount of CFRP usage and applied strengthening procedure were based on the guideline described in the "*Constructional detailing for structures*" (The Editorial Board of the Building Structural Data Set 1995). In this process, the structural adhesive glue was smeared evenly on the concrete surface then the CFRP sheets were attached to the concrete surface with fully flattening, along the fibre direction rolling compaction for several times. After completing the strengthening procedure, the specimens were stored and cured for more than 3 days under the room temperature before the tests. The completed specimens are shown in Fig. 4.

### *2.2 Loading scheme*

As shown in Figs. 5 and 6, horizontal cyclic loading scheme was adopted to carry out the tests. The servo actuator mounted on the reaction wall was connected to the end of the beam through four screws and two steel plates to apply cyclic load. The beam specimen was connected with the column (Fig. 1 and Fig. 6) in which the column was strongly bolted into the ground and horizontally jacked in position. Fig. 7 shows the locations of strain gauges on the stirrups and CFRP sheets surrounding the perforation. As shown in Fig. 8, six LVDT displacement meters were used to measure the horizontal displacement and rotation of the beam under cyclic loading.

According to Chinese Standards of "Test method of concrete structure" (Chinese State Standard 1992) and "Procedure of seismic test method for building" (Chinese Industry Standard 1996), in this research a hybrid load-displacement control loading method was adopted. As shown in Fig. 9, the details of the loading scheme are:

(1) Before the yield load was reached, the loading procedure was load control in which for each step

one cyclic load was applied.

(2) After the yield load was reached, the displacement control was adopted in which the servo actuator was reset to zero displacement. Then 5 mm of displacement increment was applied step by step (with three cycles for each step) until the load was down to 85% of the peak load.

In the rest of the paper, the positive load and displacement are referenced to the pushout force and displacement, respectively. The negative load and displacement are referenced to the pulling force and displacement, respectively (Figs. 5 and 6).

## 3. Test observations

(1) Beam LA0

LA0 was a non-perforated beam. Its failure pattern is shown in Fig. 10(a). In the test, when the beam was loaded to -9.0 kN, a crack was formed on the bottom of the beam, 150 mm away from the column. When the load was increased to -36.0 kN, an X-crack was seen, 350 mm away from the column. More cracks were appeared after further loading. When the load was increased to 50.0 kN, the specimen was yielded, after that the actuator was reset to zero and the loading scheme was switched to displacement control. At the loaded displacement $\Delta$ = -33 mm in the first cycle, the maximum resistance of the specimen was reached, that was -66.2 kN. The specimen was failed at $\Delta$=38 mm. Then the test was terminated.

(2) Beam LA1, LA2 and LA3

The perforation diameter of LA1 was 90 mm (or 0.3*h*). Its failure pattern is shown in Fig. 10(b). The first crack was appeared at the top left corner of the perforation at the load of 7.0 kN. When the load was increased to 20.0 kN, a 45° diagonal crack was formed at the left bottom corner of the perforation. The two cracks were propagated with the increasing load. When the load was reached to -23.0 kN, a 45° diagonal crack was formed on the top left edge of the perforation. The two cracks were propagated with increasing load and finally formed a large crack. When the load was reached to -36.0 kN, an X-crack was formed at 300 mm away from the edge of the column. After the load was reached to -45.0 kN (with a maximum crack width of 0.3 mm), in order to avoid sudden brittle

failure of the specimen, the displacement control loading scheme was activated. The peak resistance of -63.9 kN was reached at Δ=17 mm. The specimen failed at the second cycle of loading with Δ = -32 mm. Then the test was stopped.

The perforation diameter of LA2 was 120 mm (or 0.4*h*). Its failure pattern is shown in Fig. 10(c). The first crack, on the top of the specimen above the perforation, was appeared at a load of 5.7 kN. When the load was increased to 18.0 kN, diagonal cracks tangent to the edge of the perforation were formed. When the load was reached to -17.2 kN, 45° diagonal cracks were seen on the left top and bottom edge of the perforation. When the load was reached to -36.0 kN, the first X-crack was appeared at 300 mm away from the column edge. At the load of -55.7 kN, the crack previously appeared near the edge of the column was spread to the top edge of the perforation to form a diagonal crack. The specimen was yielded at the load of -58.8 kN then the loading scheme was shifted to displacement control. The peak load resistance of 63.0 kN was reached at Δ=19mm. The specimen failed at the second cycle of Δ=23.6 mm.

The perforation diameter of LA3 was 150 mm (or 0.5*h*). Its failure pattern is shown in Fig. 10(d). When the load was reached to -9.0 kN, a 45° diagonal crack was appeared on the bottom right edge of the perforation. More cracks were formed with further loading. At 18.0 kN, a crack was seen tangent to the top edge of the perforation. At -18.0 kN, a crack was formed tangent to the bottom edge of the perforation. The two tangent cracks were developed to be large cracks. When the load was reached to 41.3 kN, the brittle failure of the beam suddenly happened with a loud cracking sound. The brittle failure of the beam happened before shifting to displacement control stage.

It can be seen that Beams LA1, LA2 and LA3 all failed by shear at the position closed to perforation. The direction and the position of the cracks were consistently initiated tangent to the edge of the perforation and propagated later. This is due to the stress concentration after perforation, which consequently decrease the shear resistance of the beams. The bigger the perforation was, the sooner the cracks formed and propagated, and lower load resistance was.

(3) Beams LC1, LC2-1, LC2-2 and LC3

These four beams were strengthened with CFRP sheets. The perforation diameter of LC1 was

90 mm (or 0.3*h*), strengthened with CFRP sheets with horizontal arrangement. The failure pattern of LC1 is shown in Fig. 10(e). At 15.2 kN of load, a vertical crack was formed above the perforation. This crack was quickly propagated to the top edge of the perforation to form a normal crack. When the load was increased to 21.0 kN, a 45° diagonal crack was formed on the left down side of the perforation. The first X-crack appeared 550 mm away from the edge of the column when the load was reached to -45.0 kN. The specimen was yielded at the load of -51.0 kN. Then the loading was switched to the displacement control. The specimen was reached to its peak resistance of 69.3 kN at $\Delta$=31 mm. With the increase of displacement, concrete surrounding the perforation was sloughing off successively and the CFRP sheets were gradually spalled off. At $\Delta$=57 mm, the test was stopped due to the failure of the intersection between the beam and the column.

The perforation size of LC2-1 was 120 mm (or 0.4*h*), strengthened with CFRP sheets with horizontal arrangement. The failure pattern of LC2-1 is shown in Fig. 10(f). A crack appeared at the bottom of the beam when the load was increased to 14.0 kN. At 18.7 kN, a diagonal crack was formed at the bottom edge of the hole. At -27.0 kN, a crack was seen on the top left edge of the hole. At -36.0 kN, an X-crack was formed at the position of 435 mm away from the column. More cracks were formed with the further loading. At -51 kN, the beam yielded. Then the loading was switched to displacement control. The beam reached its peak resistance of 68.5 kN at the first cycle of $\Delta$=31.8 mm. Further loading caused more and more spalling of CFRP sheets and diagonal wrinkles were appeared in the sheets. When the beam was loaded to $\Delta$= -31.8 mm, the longitudinal CFRP sheet on the right of the hole was suddenly tore off. This led to the failure of the beam and the test was then stopped.

The perforation size of LC2-2 was 120 mm (or 0.4*h*) and strengthened with CFRP sheets with 45° diagonal arrangement. The failure pattern of LC2-2 is shown in Fig. 10(g). A crack appeared at the top of the hole when the load was increased to 18.0 kN. At -16.0 kN, a crack was formed at the bottom right edge of the hole. At -32.0 kN, an X-crack appeared at the position of 530 mm away from the column. A diagonal crack was also seen on the top left edge of the hole. When the beam was loaded to 45.5 kN, the 45° diagonal crack on the top right edge of the hole propagated through the CFRP sheets. The beam yielded at the load of -51 kN. Thus the loading procedure was switched

to displacement control. For the first cycle at Δ=16.5 mm, the beam reached its peak resistance of 68.3 kN. CFRP sheets were spalled off successively with further loading. At the second cycle load of Δ=26.5 mm, the sheets BZS2 and BZX2 (see Fig. 7(c) for the positions) were spalled off completely with a sudden bang. At Δ=36.5 mm, a large amount of concrete was spalled off at the left side of the hole and the anchorage of the sheets failed suddenly. The test was then stopped.

The perforation size of LC3 was 150 mm (or 0.5*h*), strengthened with CFRP sheets using horizontal arrangement. The failure pattern of LC2-2 is shown in Fig. 10(h). At 11.0 kN, cracks appeared on the left bottom edge and top edge of the hole and merged into one crack later. At -45.0 kN, an X-crack was formed at the position of 475 mm away from the column. The beam yielded at 49.9 kN. Then the loading procedure was switched to displacement control. The beam reached its peak resistance of 68.5 kN at the first cycle of Δ=14.7 mm and the CFRP sheets on the left of the hole spalled off. The beam failed at the second cycle of Δ=24.7 mm.

It is evident from the test observations that the beams strengthened with CFRP sheets could effectively restrain the cracks' development around the perforation, and hence improve the ultimate resistance and ductility of the beam. The failure of Beam LC1 happened at the junction of the beam and the column, while Beams LC2-1, LC2-2 and LC3 exhibited shear failure around the perforation. It is clear from the tests that the ductility of the beam strengthened with CFRP sheet could decrease significantly with the increased size of perforation.

## 4. Analysis of test results

Due to the limited number of the specimens tested in this research, there is no reliability analysis for the test results presented here.

### *4.1 Load resistance*

The cracking loads, ultimate loads and ultimate displacements of the beams with and without CFRP sheets strengthening, together with the non-perforated beam LA0, are given in Table 3.

It can be seen from Table 3 that the initial cracking loads of LA1 and LA2 were 7.0 kN and 5.7 kN, respectively, which were 22% and 37% lower than 9.0 kN of LA0; the normal cracking load of LA2

was 13.4 kN, which was 26% lower than 18.0 kN of LA1; the diagonal cracking loads of LA2 and LA3 were 17.2 kN and 9.0 kN, respectively, which were 14% and 55% lower than 20.0 kN of LA1. This indicates that perforation decreases the initial cracking load, and the initial, normal and diagonal cracking loads decrease with the increase of perforation size. In addition, the perforation size of LA3 was almost half of the depth of the specimen, the more significant stress concentration and greater shear stress caused the diagonal cracks appeared earlier and developed more quickly than other cracks, hence, the specimen failed without forming normal cracks.

In Table 3, the ultimate resistance of the specimens LA1, LA2 and LA3 were respectively 63.9 kN, 63.0 kN and 41.3 kN, which were 4%, 5% and 38% lower than 66.2 kN of LA0. This indicates that the resistance of the specimen to the load reduces with greater perforation.

The initial cracking loads of LC1, LC2-1 and LC3 were respectively 15.2 kN, 14.0 kN and 10.0 kN, which were 117%, 146% and 11% higher than 7.0 kN, 5.7 kN and 9.0 kN of LA1, LA2 and LA3 (without CFRP sheets strengthening ). The ultimate loads of LC1, LC2-1 and LC3 were respectively 69.3 kN, 68.5 kN and 68.5 kN，which were 8%、9%、66% higher than 63.9 kN, 63.0 kN and 41.3 kN of LA1, LA2 and LA3. The test results show that CFRP sheets' strengthening improves the initial cracking resistance and the ultimate load resistance of the beams. The CFRP sheets compensate the weakening effect of perforation and restrain the cracks from propagating, and thus effectively improve the shear resistance of the beam.

Specimen LC2-2 was strengthened with $45^{o}$ diagonal arrangements. Compared with LC2-1, strengthened with horizontal arrangement, their ultimate loads were nearly the same. However, the initial cracking load, normal cracking load and diagonal cracking load of LC2-2 were increased by 14%, 25% and 71%, respectively compared to LC2-1. This indicates that strengthening method with different arrangements has a considerable influence on the development of cracks. Compared LC2-2 with LC2-1 the strengthening method with $45^{o}$ diagonal arrangements was a more effective way to restrain the development of cracks. However, more tests are needed before general conclusions can be drawn.

### *4.2 Strain distribution in the stirrups and CFRP sheets*

Fig. 11 shows the strain distributions in the stirrups and CFRP sheets of the specimens LA1, LA2, LA3 (without strengthening) and LC1, LC2-1 and LC3 (with strengthening) under positive loading conditions. As shown in Figs. 11(a), 11(b) and 11(c) (for LC1, LC2-1 and LC3) at the same load level the strains in the stirrups besides the perforation (G1, in Fig. 7(a) for the position) were smaller than those in the CFRP sheets (B1, in Fig. 7(b)). Also it is evident that the strains in the stirrups of the specimens LA1, LA2 and LA3 were significantly great compared to the specimens strengthened with CFRP sheets. This is because of under low frequency cyclic load, the crack propagation is firstly restrained by the CFRP sheets, then the stirrups. This mechanism improves the integrity of the concrete surrounding the perforation. Hence, the shear resistance of the specimen is effectively enhanced.

Fig. 11(d) shows the influence of the perforation size on the strains in the stirrups of strengthened specimens LC1, LC2-1 and LC3. It can be seen that at the same load level, the strains in the stirrups besides the perforation were increased with the increase of perforation size. This is due to that the increase of perforation size decreases the effective concrete area to resist shear force. Hence, the crack restraining effect of CFRP sheets is reduced.

### *4.3 Hysteresis performance and energy dissipation capacity*

#### *4.3.1 Load-displacement hysteresis curves*

Fig. 12 shows the load-displacement hysteresis curves at the end of the beams. In the figure, the horizontal coordinates denote horizontal displacement $\Delta$, the vertical coordinates denote the horizontal load applied. It can be seen from Figs. 12(c), (e) and (g) that for the beams without strengthening, LA1, LA2 and LA3 (with hole diameters of 0.3$h$, 0.4$h$ and 0.5$h$), the satiation of the hysteresis curves of the beams were very significantly decreased with the increase of hole size. Also the area inside the curves was significantly shrunk. This indicates the decrease of energy dissipation capacity of the beams. The reduction of hysteresis performance is caused by the decrease of the effective beam section and the increase of stress concentration around the hole, leading to earlier spalling of the concrete.

Figs. 12(d), (f) and (h) show the hysteresis curves of LC1, LC2-1 and LC3 (with hole diameters of 0.3*h*, 0.4*h* and 0.5*h*) strengthened with CFRP sheets. It is evident that the perforation size has significant impact on the satiation of hysteresis curves and the energy dissipation capacity of the beams. Hence, the hysteresis performance of the beams is deteriorated considerably with increased perforation size, especially when the perforation is large than 0.4*h*.

The results show that the hysteresis performance of the beams with CFRP sheets strengthening is considerably improved. The reason is that the cracking of concrete is restrained from propagation by CFRP sheets and the integrity of concrete surrounding the hole is improved. Hence, the ductility and energy dissipation capacity of the beams are increased and consequently the seismic performance of the beams is enhanced.

Compared Beams LC2-2 (strengthened with diagonal arrangement) and LC2-1(strengthened with horizontal arrangement), it can be seen from Figs. 12(b) and (f) that the satiations of hysteresis curves are similar, with almost the same enclosure area. This indicates that both beams have the similar energy dissipation capacity.

*4.3.2 Relative rotation of the beam*

Two LVDTs were installed (Fig. 8) to measure the relative displacement of the beam and the column for calculating the relative rotation (Dai and Yuan 2005). The calculated ultimate relative rotations of the beams are given in Table 4.

It can be seen from Table 4 that the ultimate relative rotations of the perforated beams (LA1, LA2 and LA3) were smaller than those of unperforated beam LA0. The ultimate relative rotations of LA1, LA2 and LA3 were 73%, 47% and 18% of that of LA0, respectively. This indicates that the relative rotation of the beam decreases with perforation size.

It is also known from Table 4 that the ultimate relative rotations of LC1, LC2-1 and LC3 were 103%, 53% and 149% larger than that of LA1, LA2 and LA3, respectively. This indicates that the beams strengthened with CFRP sheets have more ultimate relative rotation capacity. The use of CFRP sheets can effectively restrain the crack propagation around the hole and improve the

ductility and integrity of the perforated beams. In addition, the ultimate relative rotations of LC1, LC2-1 and LC3 were decreased significantly with the increase of the hole size. Therefore, based on the ultimate relative rotation and ultimate load, the perforation size should be limited, not exceeding 0.4*h*. The ultimate relative rotation of LC2-2 was 0.044, 29% larger than 0.035 of LC2-1. According to Fig. 12 (also see Table 5), the ultimate displacement for both specimens "LC2-1" and "LC2-2" is nearly the same. Hence, the higher ultimate relative rotation of LC2-2 compared to LC2-1 may indicate the concentration of damage near the beam-column connection in specimen LC2-2 while for specimen LC2-1 the damage was distributed more evenly. This further indicates that the strengthening method with different arrangements has a considerable influence on the development of cracks.

*4.3.3 Energy dissipation capacity*

Under low frequency cyclic load, the amount of energy dissipated in one load cycle can be represented as the encompassed area of the load-displacement hysteresis curve in that cycle (Structural Engineers Association of California 1995). The energy dissipation capacity in each load cycle can be represented by the relationship between the area of the first hysteresis loop and the peak displacement $\Delta$ in that loop. Fig. 13 shows the energy dissipation capacity of the beams.

It can be seen from Figs. 13(a), (b) and (c) that, at the same displacement, energy dissipation capacities of Beams LC1, LC2-1 and LC3 (with strengthening) are higher than Beams LA1, LA2 and LA3 (without strengthening). As shown in Fig. 13(b), Beams LC2-1and LC2-2 have nearly the same energy dissipation capacities. This indicates that the two strengthening methods have the similar energy dissipation capacity. Fig. 13(d) shows the influence of the perforation size on the energy dissipation capacity of the beams. It can be seen that energy dissipation capacity decreases considerably with increase of the perforation size of beams. For the beams with the perforation size less than 0.4*h*, the energy dissipation capacity of strengthened perforated beams is comparable to non-perforated beam LA0. Hence, it is better to limit the size of perforation less than 0.4*h*.

### *4.4 Ductility*

In this study, the displacement ductility coefficient (Chinese State Standard 2010) is used to estimate the ductility of the beams. The displacement ductility coefficients calculated from the test results are given in Table 5.

The ductility coefficients of strengthened Beams LC1, LC2-1 and LC3 were 59%, 79% and 117% larger than that of LA1, LA2 and LA3, respectively. This demonstrates that CFRP sheets' strengthening could effectively improve the ductility of perforated beams. Compared to non-perforated beam LA0 the ductility coefficients of LC1, LC2-1, LC3, and LC2-2 were increased by 129%, 84%, 62% and 85%, respectively. Also it can be seen that large perforation size (>0.4$h$) decreases the ductility of strengthened beams considerably. Therefore, in engineering practice it seems reasonable to limit the perforation size less than 0.4$h$. It is also noted that both strengthening methods (LC2-1 and LC2-2) has the similar effect on the ductility of the beam.

### *4.5 Stiffness degradation*

In this paper the change of the equivalent stiffness $K$ of the beams under cyclic load is used to evaluate the stiffness degradation (Yin 1995) of beams. Fig. 14 shows the relationships between equivalent stiffness $K$ and the average displacement $\Delta$ of the beams.

It can be seen from Fig. 14 that, under cyclic loads, the stiffness of the beams was degraded significantly, which was mainly caused by the development of cracking in the concrete surrounding the hole. As shown in Figs 14(a), (b) and (c), the initial stiffness of strengthened Beams LC1, LC2-1 and LC3 was greater than that of Beams LA1, LA2 and LA3 (without strengthening). This indicates that the stiffness of the beam was enhanced by the strengthening with CFRP sheets. The stiffness of the beams was decreased quickly under low frequency cyclic loading. However, the crack propagation in the concrete was restrained by CFRP sheets so that the stiffness degradation of Beams LC1, LC2-1 and LC3 was lagged behind Beams LA1, LA2 and LA3. With further loading the beams entered plastic stage. In the plastic stage, the stiffness degradation of the beams was slowed down, exhibiting gradually reduced slope of the curve.

In the period, nearly reaching the ultimate load capacity of the specimen, the stiffness degradation was almost proportional to the displacement increment. As shown in the figure, the stiffness of the strengthened beams was always greater and declined slower than that of the beams without strengthening. As shown in Fig. 14(b) the stiffness degradation curves of LC2-1 and LC2-2 coincided with each other. That means there is not much difference between the two strengthening methods for improving the stiffness of the beams. Fig. 14(d) shows that the initial stiffness of LC1 and LC2-1 was greater than that of LA0. However, the initial stiffness of LC3 was considerably lower than that of LA0. This indicates that for large perforation size (>0.4*h*), the stiffness loss caused by the large perforation cannot be compensated by strengthening with CFRP sheets. Therefore, it is suggested that the perforation size should not be more than 0.4*h* in engineering practice.

## 5. Conclusions

In this research, eight end-perforated RC frame beams with the three different sizes of perforations and two arrangement styles of the strengthening carbon fibre (CFRP) sheets were tested to assess their seismic performance using hybrid load-displacement control loading method. From the test results and observations some conclusions can be drawn as:

(1) The cracking loads of the perforated beams strengthened with CFRP sheets can be effectively enhanced. The initial cracking loads of the specimens with CFRP sheets' strengthening are 2 to 2.5 times compared to the specimens without strengthening. However, the cracking load decreases considerably with the increase of perforation size.

(2) The perforated beams strengthened with CFRP sheets can effectively increase their ultimate load capacity up to 10%. After cracking of concrete surrounding the hole, CFRP sheets come into play before steel stirrups and restrain the propagation of cracks to improve the integrity and shear resistance of the beam.

(3) Compared to the perforated beams without strengthening, the displacement ductility coefficient of the specimens strengthened with CFRP sheets is increased from 60% to more than 100%. Hence, the seismic performance of the perforated beams with CFRP sheets

strengthening around the hole can be significant improved in terms of hysteresis performance, energy dissipation capacity, ductility, and stiffness degradation.

(4) Strengthening methods with horizontal and 45° diagonal arrangements have almost the same effects for improving hysteresis performance, energy dissipation capacity and ductility of perforated beams. However, 45° diagonal arrangement is better in restraining the propagation of cracks. Therefore, strengthening with 45° diagonal arrangement method is recommended to be adopted in engineering practice.

(5) Perforation size of beam has significant influence on its seismic performance. With the increase of hole diameter, the hysteresis performance, energy dissipation capacity and ductility of beams are decreased considerably. Comparing the results of the specimens with and without CFRP strengthening, it can be seen that the strengthening with CFRP sheets is more efficient for weaker specimens (as the opening size increases, the effect of CFRP sheets increases too). However the overall performance of beams with great perforation is not desirable even with the improving effect of CFRP sheets. Therefore, it is suggested that the perforation size should not exceed 0.4$h$ in engineering practice.

## Acknowledgements

This research was supported by the Jiangsu Collaborative Innovation Centre for Building Energy Saving and Construction Technology (NO. SJXTQ 1613), Natural Science Foundation of Jiangsu Province (Grant No. BK20170282) and the Research Fund for Doctoral Program of Higher Education of China (Grant No. 2016M601911). The authors gratefully appreciate the supports.

## References

Ahmed A, Fayyadh MM, Naganathan S, Nasharuddin K (2012) Reinforced concrete beams with web openings: A state of the art review. *Materials & Design* **40**: 90-102.

Anil O (2008) Strengthening of RC T-section beams with low strength concrete using CFRP composites subjected to cyclic load. *Construction and Building Materials* **22(12)**: 2355–2368.

Aykac B, Aykac S, Kalkan I, Dundar B, Can H (2014) Flexural behavior and strength of reinforced concrete beams with multiple transverse openings. *ACI Structural Journal*, **111(2)**: 267-277.

Chinese State Standard (1992) *GB50152-92: Standard methods for testing of concrete*

*structures.* China Building Industry Press, Beijing.

Chinese Industry Standard (1996) *JGJ101—96: Specification of testing method for earthquake resistant building.* China Building Industry Press, Beijing.

Chinese State Standard (2010) *GB5011-2010, Code for seismic design of buildings.* China Building Industry Press, Beijing.

Dai K and Yuan Y (2005) Experimental study on seismic behavior of corroded frame edge joints. *Journal of China University of Mining and Technology* **34(1)**: 51-56.

Douglas TR and Gambrell SC (1974) Design of beams with off-center web openings. *Journal of the Structural Division, ASCE* **100(NST6)**: 1189-1203.

El-Maaddawy T and El-Ariss B (2012) Behavior of concrete beams with short shear span and web opening strengthened in shear with CFRP composites. *Journal of Composites for Construction* **16(1)**: 47-59.

Grace NF and Ross B (1996) Dynamic characteristics of post-tensioned girders with web openings. *Journal of Structural Engineering ASCE* **122(6)**: 643-650.

Mansur MA, Tan KH, Lee SL (1985) Design method for reinforced concrete beams with large openings. *Journal of the American Concrete* **82(4)**: 517-524.

Mansur MA, Lee Y F, Lee S L (1991) Tests on RC continuous beams with openings. *Journal of Structural Engineering ASCE* **117(6)**: 1593—1606.

Structural Engineers Association of California (1995). *SEAOC Version 2000: Performance based seismic engineering of buildings: Conceptual Framework.* Sacramento (CA).

The editorial board of the Building structural data set (1995) *Building structural data set.* China Building Industry Press.

Wang F, Li Z, Cui H (2011) Experimental study on mechanical properties of reinforced concrete frame beams with openings in the end. *Engineering Mechanics* **28(11)**: 52-58.

Xue H and Zheng L (2014) Numerical simulation on the form of reinforcement of reinforced concrete beam with openings. *Applied Mechanics and Materials* **444-445**: 884-888.

Yin Z. (1995) Seismic behavior and design method of reinforced concrete circular hole beams. *Journal of Building Structures* **16(2)**: 18-32.

Zhang ZC and Hsu CTT (2005) Shear strengthening of reinforced concrete beams using carbon-fiber-reinforced polymer laminates. *Journal of Composites for Construction* **9(2)**: 158-169.

**List of Tables and Figures**

Table 1 List of beam specimens.

| Group | Specimen number | Diameter of perforation, $d$ （mm） | Distance between the edge of the perforation to the edge of the specimen, $S_1$ (mm) | Strengthening method |
|---|---|---|---|---|
| A | LA0 | - | - | - |
| | LA1 | 90（0.3$h$） | 150（0.5$h$） | None |
| | LA2 | 120（0.4$h$） | 150（0.5$h$） | None |
| | LA3 | 150（0.5$h$） | 150（0.5$h$） | None |
| B | LC1 | 90（0.3$h$） | 150（0.5 $h$） | CFRP (horizontal) |
| | LC2-1 | 120（0.4$h$） | 150（0.5 $h$） | CFRP (horizontal) |
| | LC2-2 | 120（0.4$h$） | 150（0.5 $h$） | CFRP (diagonal) |
| | LC3 | 150（0.5$h$） | 150（0.5 $h$） | CFRP (horizontal) |

Notes: $h$ is cross-section height of the beam ($h$ = 300 mm)

Table 2 Properties of steel reinforcement.

| Steel bar | Type | Diameter (mm) | Yield strength $f_{yk}$ ( $N/mm^2$ ) | Ultimate strength $f_{uk}$ ( $N/mm^2$ ) |
|---|---|---|---|---|
| Stirrup (Tie) | HPB300 | 6 | 347.0 | 482.7 |
| Main steel bar | HRB400 | 18 | 499.0 | 640.0 |

Table 3 List of cracking loads, ultimate loads and displacements of the specimens.

| Label | Cracking load (kN) | | | Ultimate load (kN) | Ultimate displacement (mm) |
|---|---|---|---|---|---|
| | Initial crack at the edge of the beam | Normal crack at the edge of the hole | Diagonal crack around the hole | | |
| LA0 | 9.0 | — | — | 66.2 | 38.0 |
| LA1 | 7.0 | 18.0 | 20.0 | 63.9 | 35.5 |
| LA2 | 5.7 | 13.4 | 17.2 | 63.0 | 22.6 |
| LA3 | — | — | 9.0 | 41.3 | 12.0 |
| LC1 | 15.2 | 18.0 | 21.0 | 69.3 | 56.5 |
| LC2-1 | 14.0 | 16.0 | 18.7 | 68.5 | 34.1 |
| LC2-2 | 16.0 | 20.0 | 32.0 | 68.3 | 24.3 |
| LC3 | — | 10.0 | 11.0 | 68.5 | 36.1 |

Table 4 The ultimate relative rotation of strengthened beam specimens.

| Specimen number | Ultimate relative rotation (radian) |
|---|---|
| LA0 | 0.049 |
| LA1 | 0.036 |
| LA2 | 0.023 |
| LA3 | 0.009 |
| LC1 | 0.072 |
| LC2-1 | 0.035 |
| LC3 | 0.022 |
| LC2-2 | 0.045 |

Table 5 Ductility coefficients calculated from the test results.

| Specimen | Yield displacement, $\Delta_y$ (mm) | Ultimate displacement, $\Delta_u$ (mm) | Displacement ductility coefficient, $\mu_\Delta$ |
|---|---|---|---|
| LA0 | 9.3 | 38.0 | 4.1 |
| LA1 | 10.8 | 35.5 | 3.3 |
| LA2 | 11.7 | 22.6 | 1.9 |
| LA3 | 10.2 | 12.0 | 1.2 |
| LC1 | 10.7 | 56.5 | 5.3 |
| LC2-1 | 9.9 | 34.1 | 3.5 |
| LC3 | 9.5 | 24.3 | 2.6 |
| LC2-2 | 10.3 | 36.1 | 3.5 |

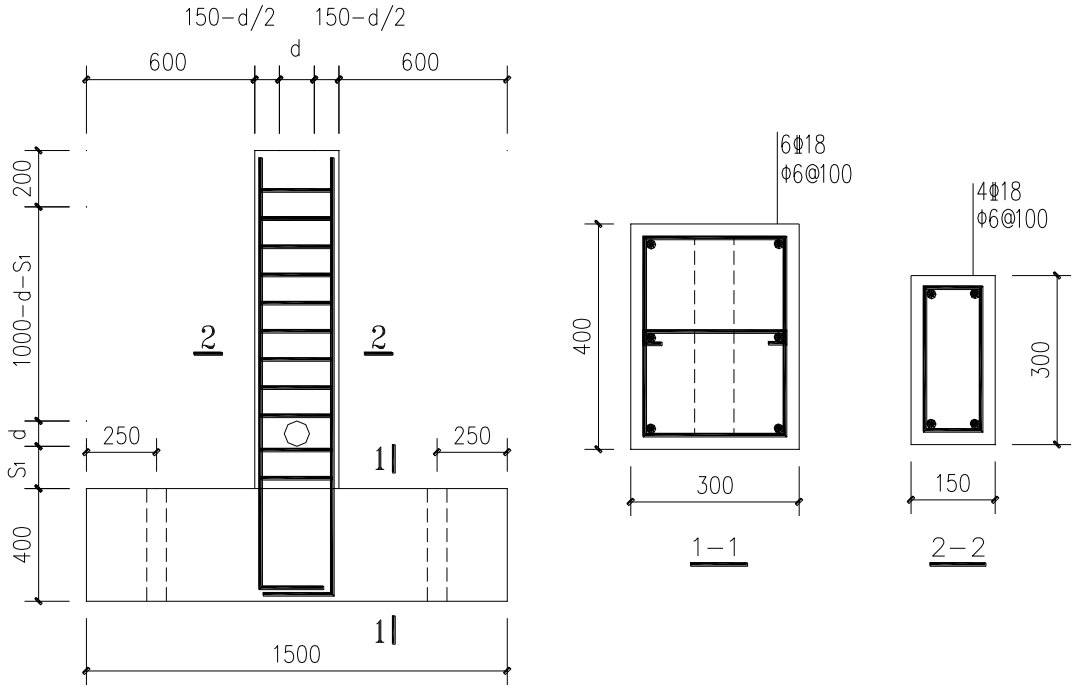


Fig. 1 Details of the perforated beams (all dimensions in mm).

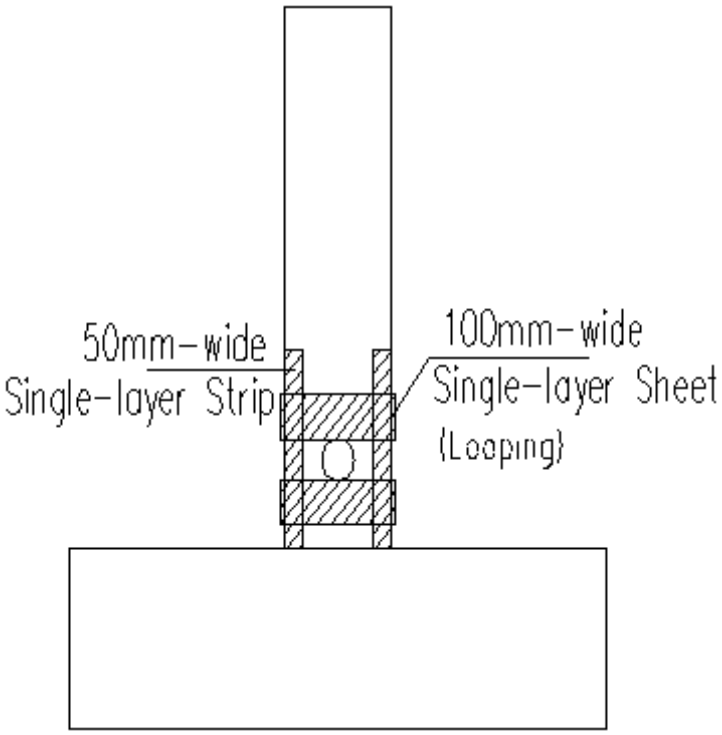


Fig. 2 Strengthening method with horizontal arrangement (Beams LC1, LC2-1, LC3).

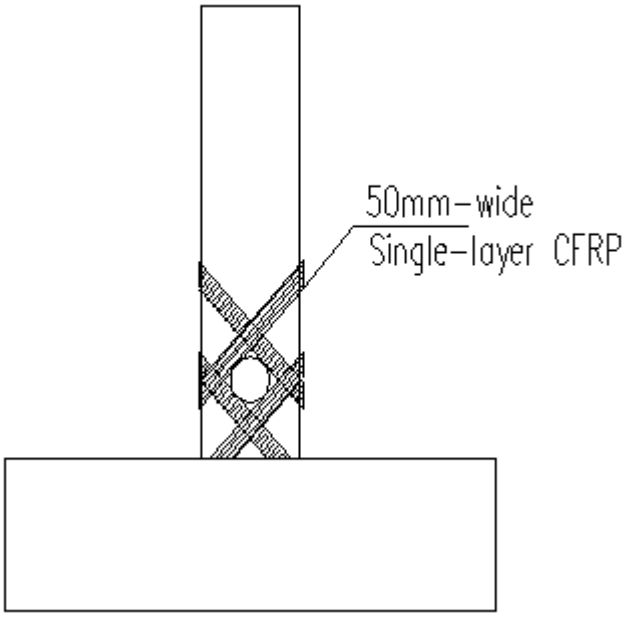


Fig. 3 Strengthening method with 45° diagonal arrangement (Beam LC2-2).

(a) Strengthening with horizontal arrangement

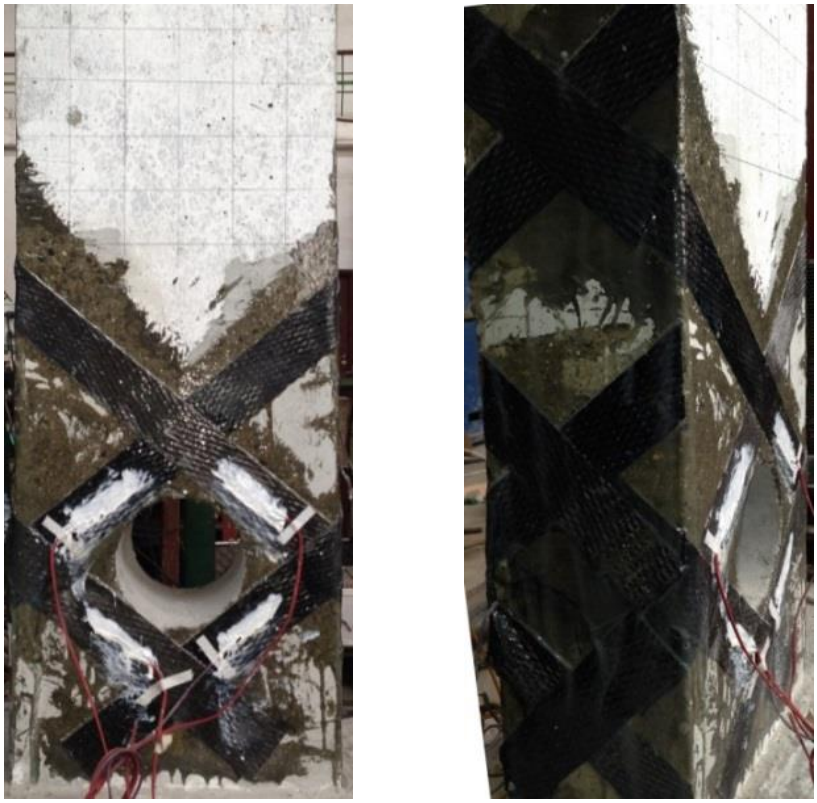

(b) Strengthening with 45° diagonal arrangement

Fig. 4 Two strengthening methods for the perforated beams.

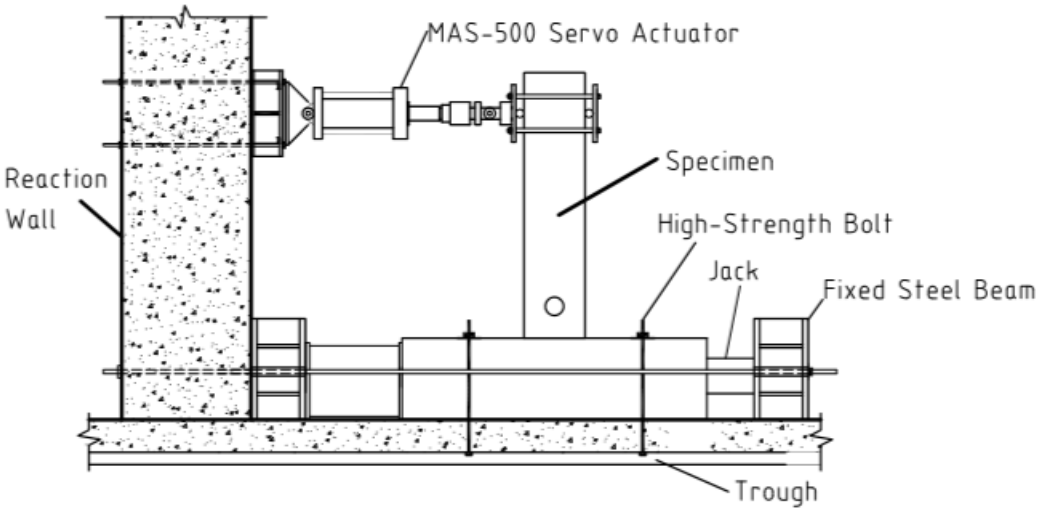


Fig. 5 Loading set up for the tests.

Fig. 6 Panorama view of the test.

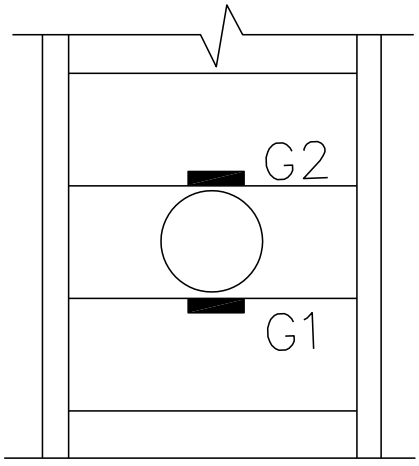


(a)

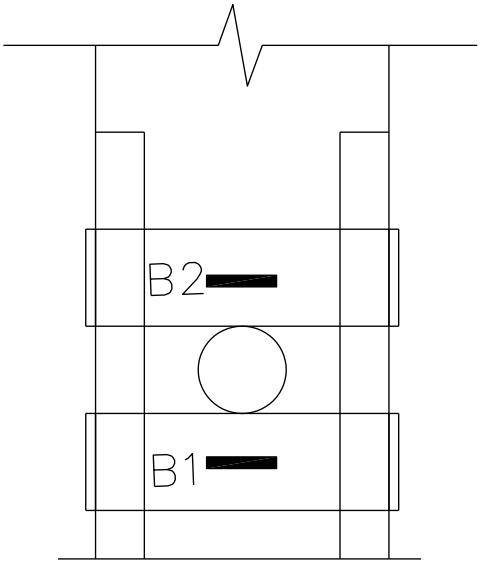


(b)

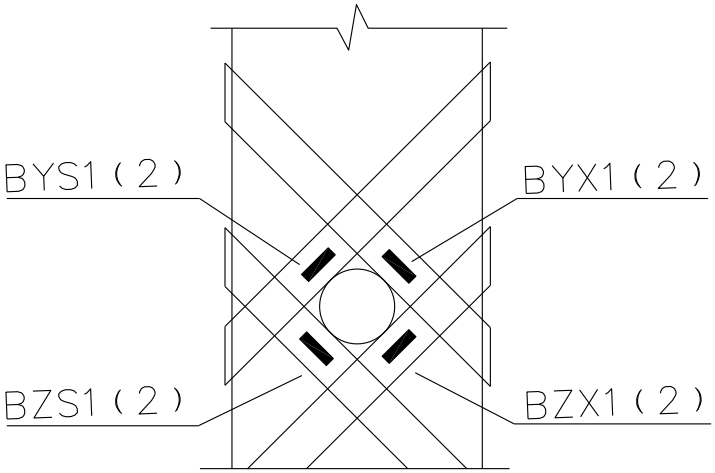


(c)

Fig. 7 Layout of strain gauges: (a) strain gauges on stirrups; (b) strain gauges on CFRP sheets (horizontal arrangement); (c) strain gauges on CFRP sheets (diagonal arrangement).

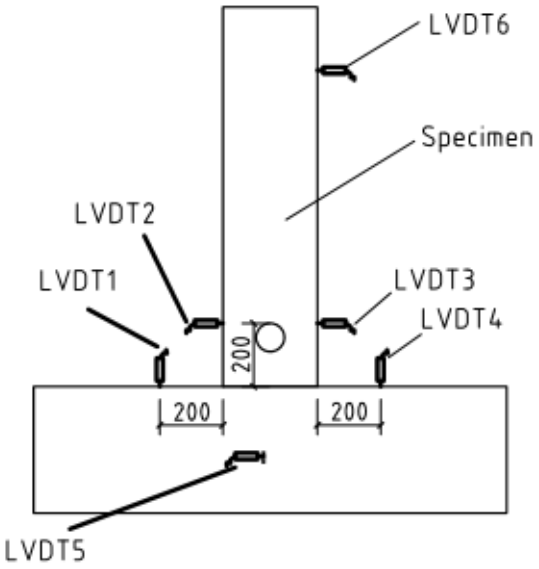


Fig. 8 Locations of LVDTs for displacement measurement.

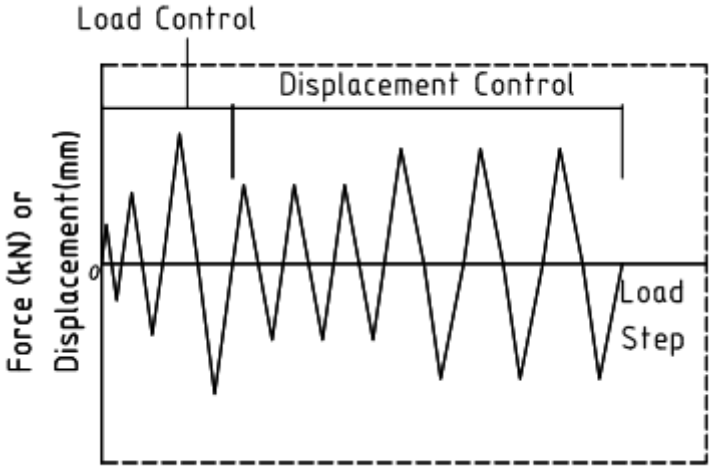


Fig. 9 Loading scheme.

**(a) LA0**

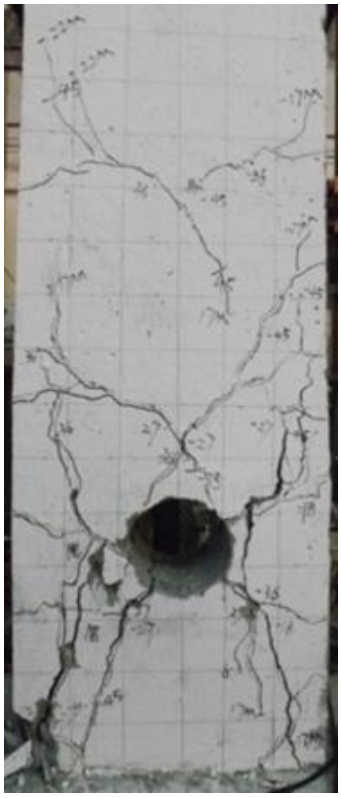

**(b) LA1**

**(c) LA2**

**(d) LA3**

**(e) LC1**

**(f) LC2-1**

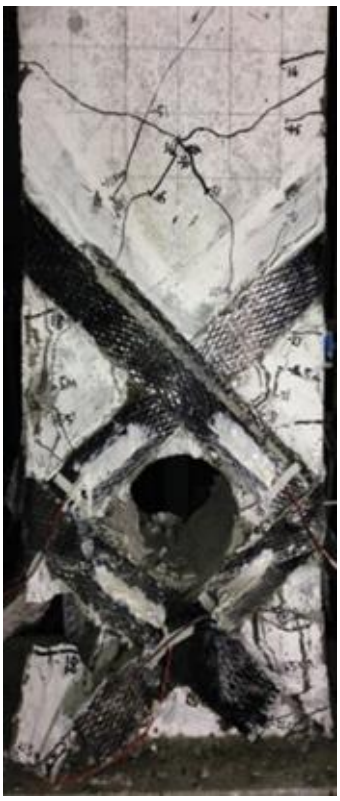

**(g) LC2-2**

**(h) LC3**

Fig. 10 Failure patterns of the specimens.

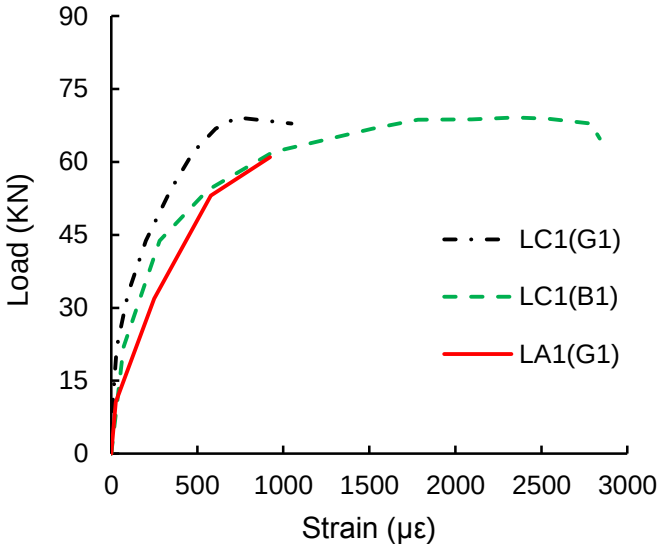
90
75
60
45
30
15
0
Load (KN)
0
500
1000
1500
2000
2500
3000
Strain (με)
LC1(G1)
LC1(B1)
LA1(G1)

**(a)**

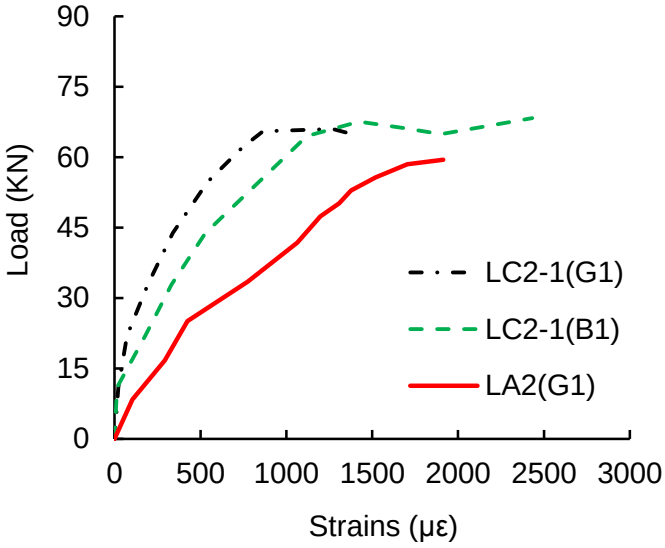
90
75
60
45
30
15
0
Load (KN)
0
500
1000
1500
2000
2500
3000
Strains (με)
LC2-1(G1)
LC2-1(B1)
LA2(G1)

**(b)**

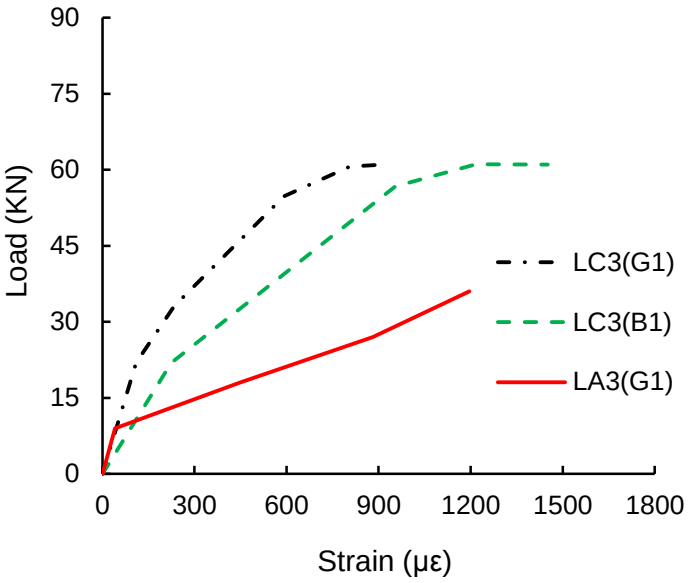


**(c)**

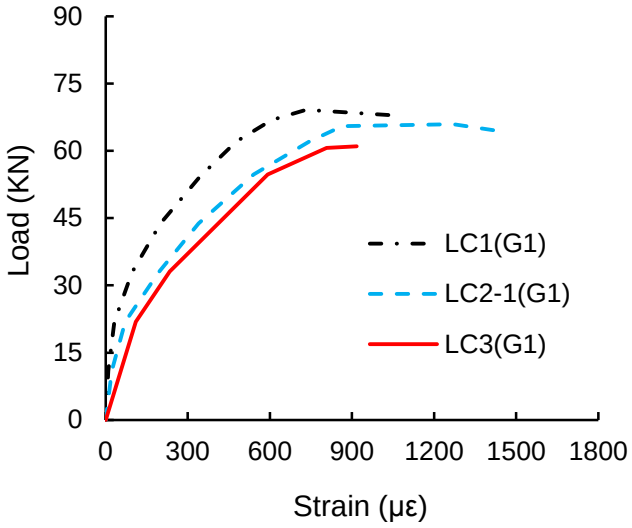


**(d)**

Fig. 11 Strains in the stirrup at G1 and CFRP sheets at B1 under positive loading (see Fig. 7 for G1 and B1 positions).

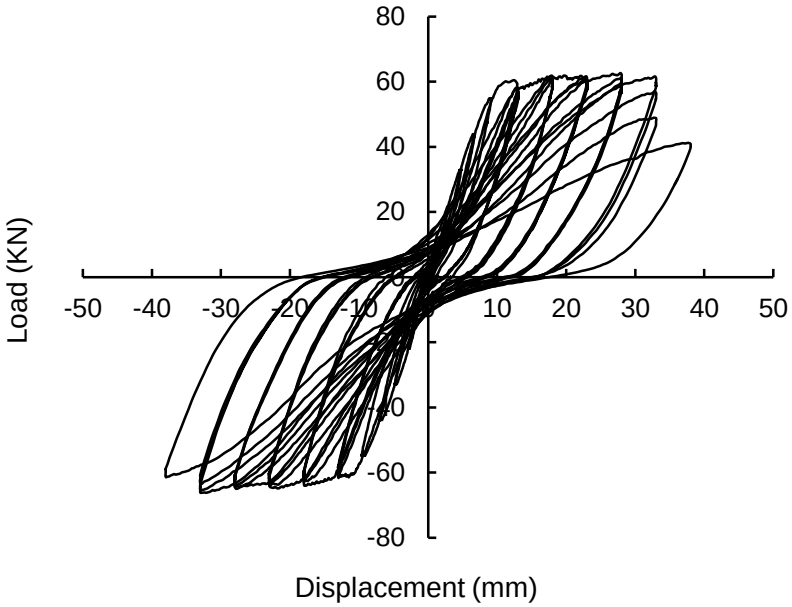


(a) Specimen LA0

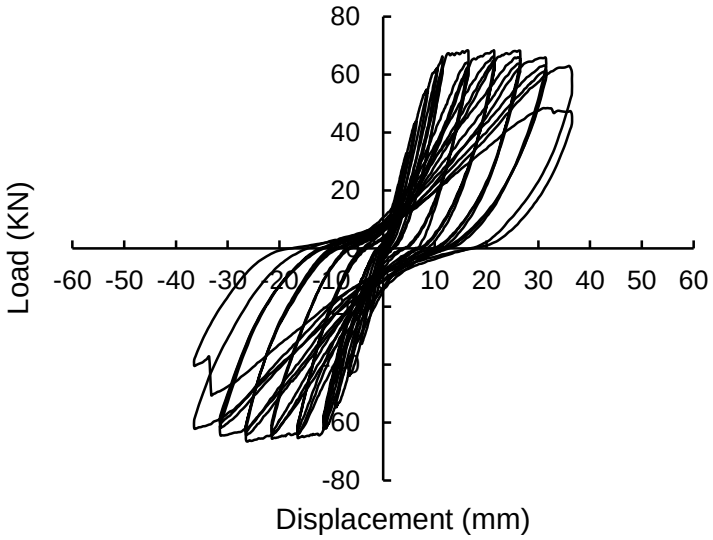


(b) Specimen LC2-2

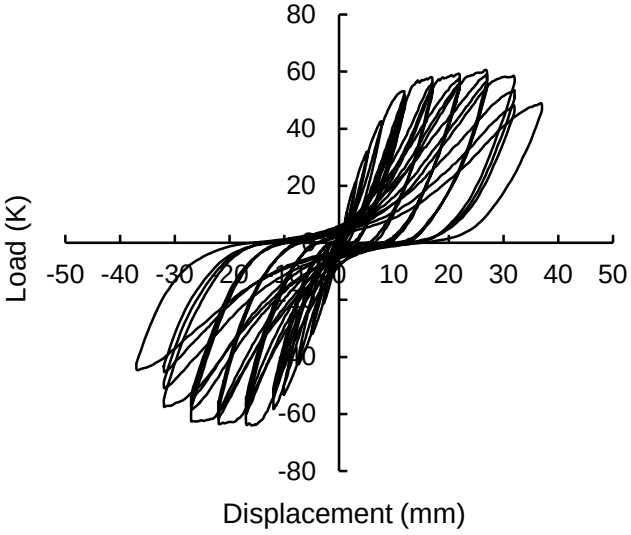


(c) Specimen LA1

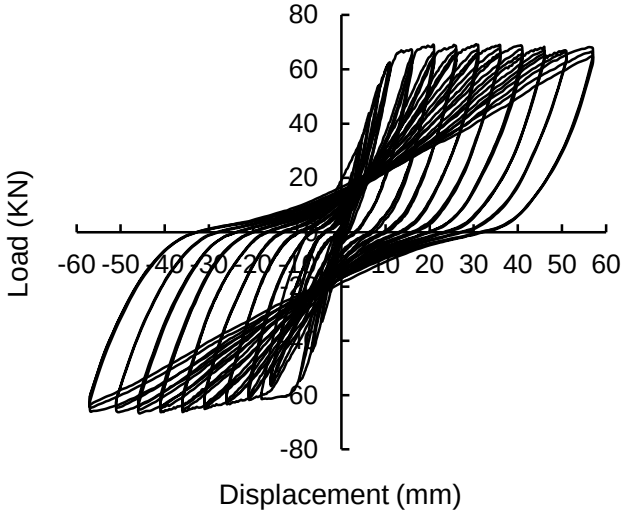


(d) Specimen LC1

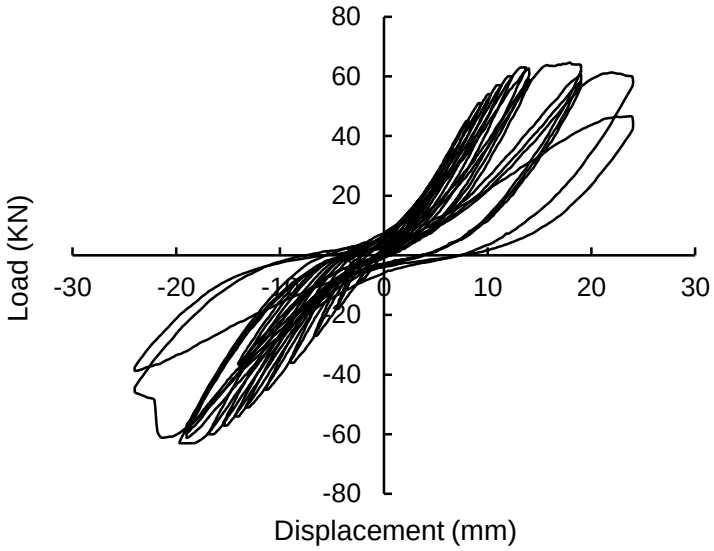


(e) Specimen LA2

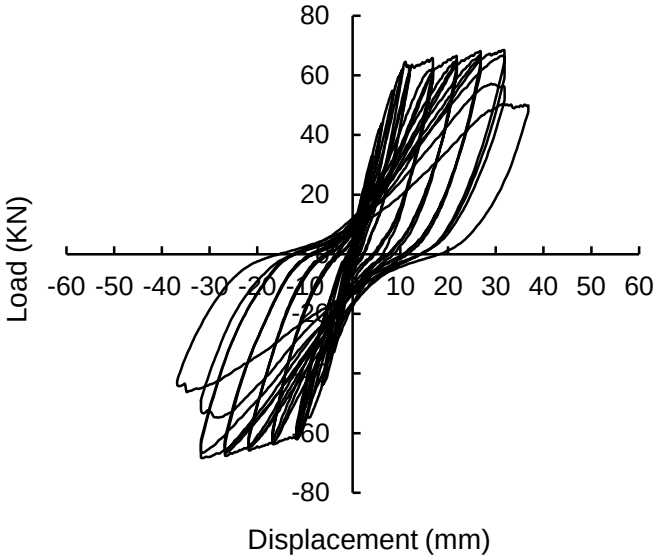


(f) Specimen LC2-1

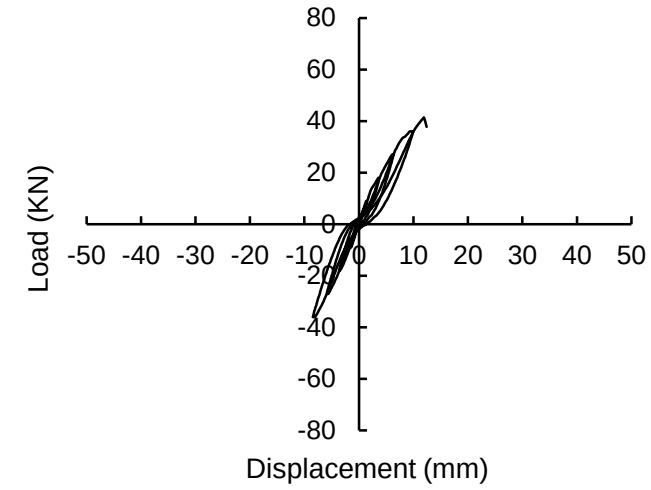


(g) Specimen LA3

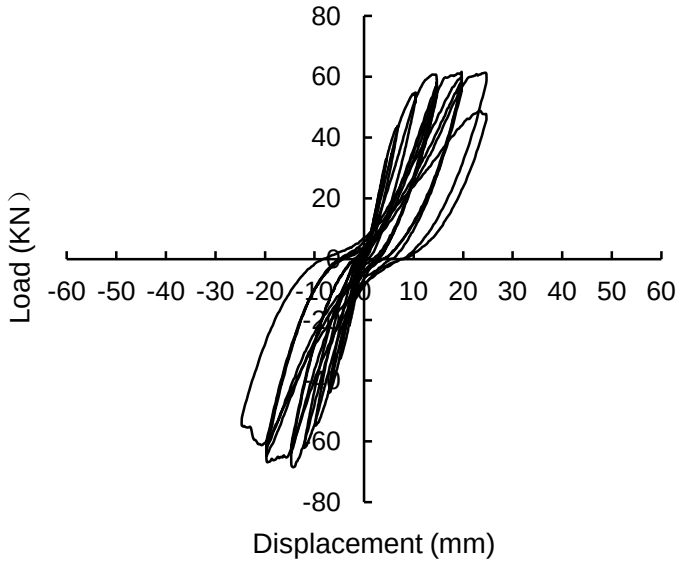


(h) Specimen LC3

Fig. 12 Load-displacement hysteresis curves of the beam specimens.

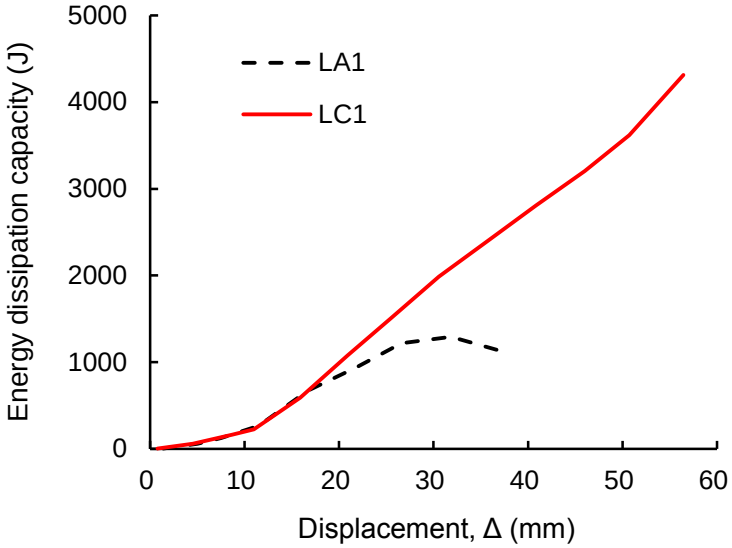
Energy dissipation capacity (J)
5000
4000
3000
2000
1000
0
0
10
20
30
40
50
60
Displacement, Δ (mm)
LA1
LC1

(a)

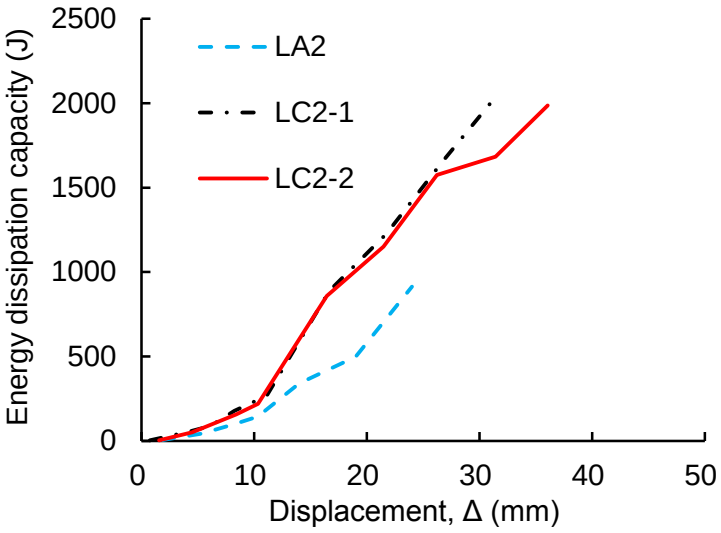
Energy dissipation capacity (J)
2500
2000
1500
1000
500
0
0
10
20
30
40
50
Displacement, Δ (mm)
LA2
LC2-1
LC2-2

(b)

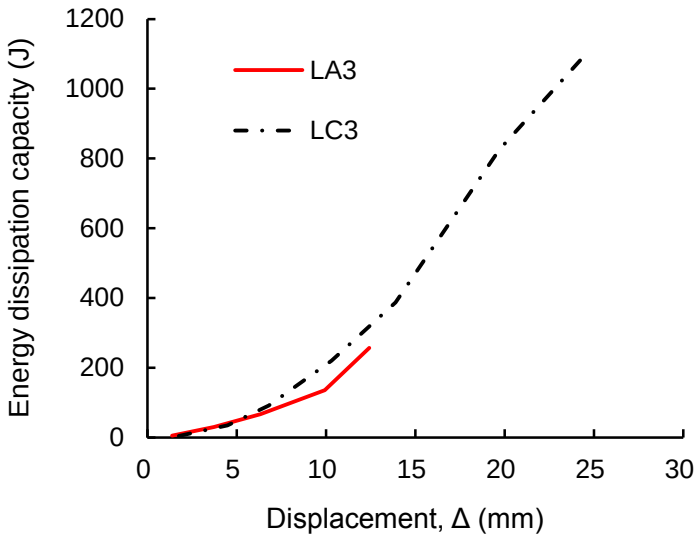


(c)

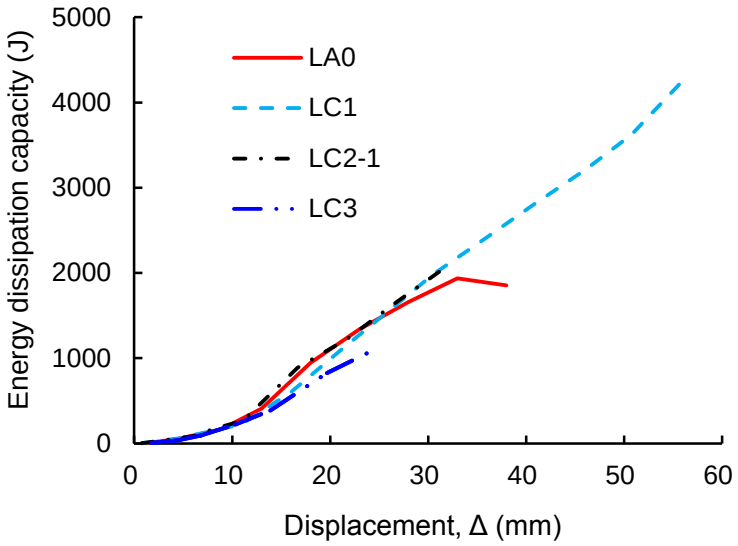


(d)

Fig. 13 Energy dissipation capacity of the beams.

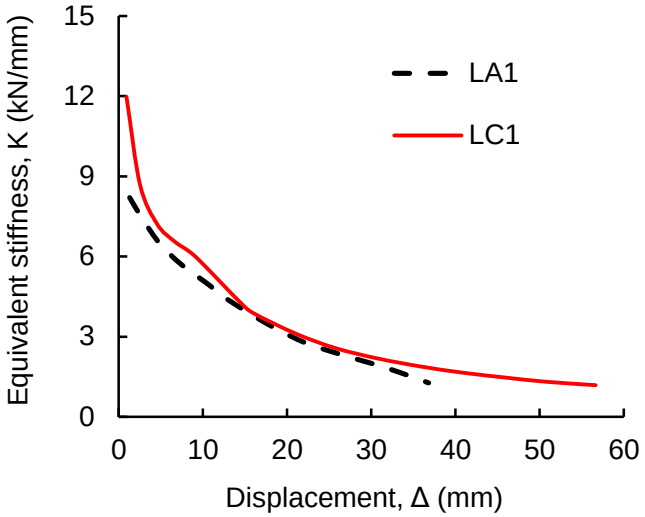
Equivalent stiffness, K (kN/mm)
15
12
9
6
3
0
0
10
20
30
40
50
60
Displacement, Δ (mm)
LA1
LC1

(a)

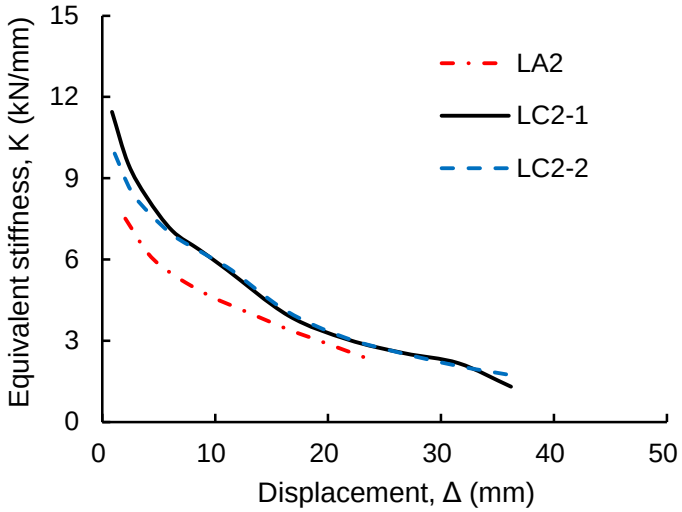
Equivalent stiffness, K (kN/mm)
15
12
9
6
3
0
0
10
20
30
40
50
Displacement, Δ (mm)
LA2
LC2-1
LC2-2

(b)

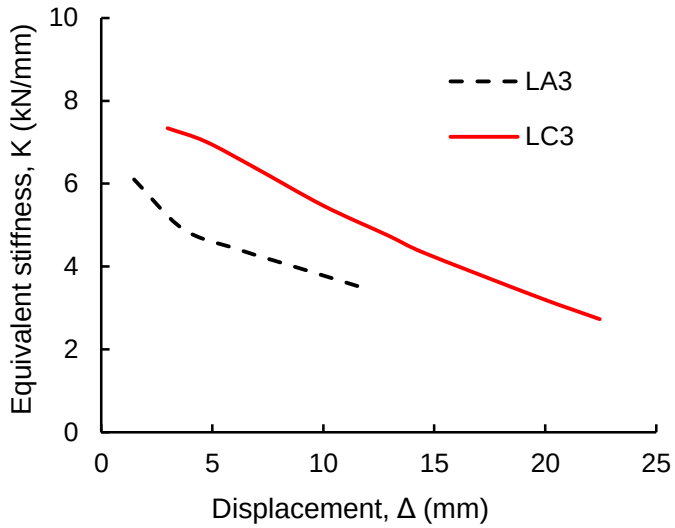


(c)

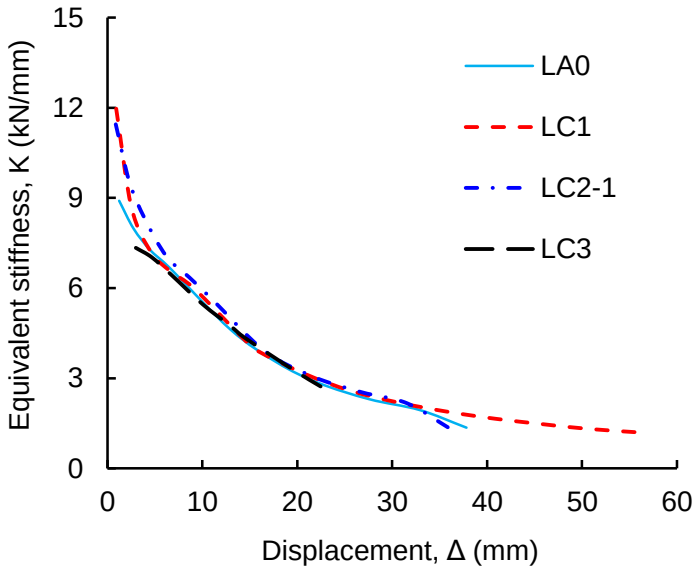


(d)

Fig.14 Stiffness degradation of the beams under cyclic load.